PNAS
www.pnas.org

Supplementary Information for

Scleral hypoxia is a target for myopia control

Hao Wu, Wei Chen, Fei Zhao, Qingyi Zhou, Peter S. Reinach, Lili Deng, Li Ma, Shumeng Luo, Nethrajeith Srinivasalu, Miaozhen Pan, Yang Hu, Xiaomeng Pei, Jing Sun, Ran Ren, Yinghui Xiong, Zhonglou Zhou, Sen Zhang, Geng Tian, Jianhuo Fang, Lina Zhang, Jidong Lang, Deng Wu, Changqing Zeng, Jia Qu, Xiangtian Zhou

Xiangtian Zhou, Jia Qu, Changqing Zeng.

Xiangtian Zhou, zxt@mail.eye.ac.cn; jqu@wmu.edu.cn; czeng@big.ac.cn.

This PDF file includes:

SI Materials and Methods

Figs. S1 to S12

Tables S1 to S8

References for SI reference citations

www.pnas.org/cgi/doi/10.1073/pnas.1721443115

SI Materials and Methods

Experimental myopia and ocular biometric measurements

Male C57BL/6 mice, about 3 weeks old, were obtained from Beijing Vital River Laboratory Animal Technology Co., Ltd. (Beijing, China) and Shanghai SLAC Laboratory Animal Co., Ltd (Shanghai, China), Mice were raised in standard mouse cages with a 12h:12h light-dark cycle at Tsing Hua University and at the Wenzhou Medical University. For both eyes of each mouse, refraction was measured by an eccentric infrared photorefractor (1), and those with an interocular difference of <3.00 diopters (D) were selected for the study. Ocular biometrics was measured by optical coherence tomography (2). Monocular form-deprivation (FD) myopia was induced by gluing a translucent occluder over the right eye, designated as the FD eye (1). The contralateral eye was untreated and designated as the control eye. Mice that failed to develop myopia were eliminated, as were those with any ocular inflammation.

Three-week-old guinea pigs (Cavia porcellus, the English short hair stock, Bikai Experimental Animal Farm, Jiangsu, China) were subjected to monocular visual manipulation with either a negative lens (-4.00 D) or a latex facemask worn over one eye to establish a lens-induction (LI) or FD myopic model, respectively (3, 4). Recovery from LI or FD was performed by removal of facemask or lens from the eye. These animals were raised with a 12h:12h light-dark cycle at Wenzhou Medical University. Refraction of each eye was measured by an eccentric infrared photorefractor while ocular axial length and vitreous chamber depth were measured by A-scan ultrasonography (3, 5). Only animals with anisometropia of less than 2.00 D were used.

Drug preparation and *in vivo* injection

To determine the effect of anti-hypoxic drugs on myopia development, we chose two compounds, salidroside with a purity of ⩾99.4% (National Institutes for Food and Drug Control, Beijing, China) and formononetin with a purity of ⩾99.0% (Sigma). Each guinea pig received unilateral injections (100 μl in the inferior periocular region) of these drugs daily for 4 weeks. Salidroside, dissolved in normal saline, was injected at low and high dosages of 1 μg per eye and 10 μg per eye respectively, with normal saline injections used as a vehicle control. Formononetin was dissolved in 0.1% dimethyl sulfoxide (DMSO) and injected at either 0.5 μg per eye or 5.0 μg per eye, with DMSO serving as a vehicle control.

To determine the individual roles of eIF2 and mTOR signaling in mediating changes in the refractive state of mice, GSK2606414 (an eIF2α kinase PERK inhibitor), salubrinal (an eIF2α dephosphorylation inhibitor), everolimus (a mTOR inhibitor), and MHY1485 (a mTOR phosphorylation activator) (all from Selleck, Shanghai, China) were administered intraperitoneally in mice as follows: GSK2606414 (100 or 330 μg/kg body weight) or everolimus (200 or 2,000 μg/kg body weight) was injected daily in FD mice for 2 weeks. Salubrinal (100 or 330 μg/kg body weight) or MHY1485 (66 or 200 μg/kg body weight) were injected daily in normal mice for 2 weeks. Mice injected with 1% DMSO served as vehicle controls. Ocular refraction was measured before and after drug injections.

scRNA-seq procedure

After 2 days of FD, the mice were euthanized by cervical dislocation, both eyes were enucleated and the sclera was isolated for single cell suspension preparation. As individual scleral tissues provided insufficient yields of cells, sclera from FD or control eyes of 6-8 mice were pooled and subsequently digested to obtain a single cell suspension. Briefly, the sclera was cut into small pieces and incubated in Dulbecco's modified Eagle's medium (DMEM) containing 0.15% (wt/vol) of type I collagenase (Sigma,) and 0.25% (wt/vol) of trypsin (Gibco) for 1 h in an incubator at 37℃ containing 5% CO_2. The solution was neutralized with 10% fetal calf serum and 0.02% ethylenediaminetetraacetic acid and filtered through a 35-μm cell strainer (BD Biosciences) and the filtrate was collected. After washing and centrifuging, the single cells were re-suspended in DMEM at concentrations of $1x10^5$ to $2x10^5$ cells/ml.

An automated microfluidic platform (Fluidigm C1 System, Fluidigm) was used to capture and lyse individual scleral cells, reverse transcribe the RNA and amplify the resulting cDNA according to manufacturer's recommended protocol. Briefly, individual scleral cells were captured on a small-size (5-10 μm cell diameter) microfluidic RNA-seq chip (C1™ Single-Cell Auto Prep IFC for mRNA, 100-5759, Fluidigm) using the Fluidigm C1 System. Cells were loaded onto the chip at a concentration of 60-180 cells/μl and imaged by a phase-contrast microscope to assess the number of cells per capture site. Only single cells were included in the analysis. The cDNA was then prepared on the chip using SMARTer Ultra Low RNA kit for Illumina (Clontech). After which, Qubit™ 1.0 Fluorometer (Invitrogen, Life Technologies) was used to calculate the concentration of each sample and a 2100 Bioanalyzer (Agilent) evaluated the quality.

Single-cell libraries were constructed in 96-well plates using the Nextera XT DNA Sample Preparation Kit (Illumina) (6). For each Fluidigm C1 experiment, bulk tissue RNA controls containing thousands of cells were processed in parallel, using the same reagents as those used on the chip. Libraries were quantified with the Agilent Bioanalyzer, using a high sensitivity DNA analysis kit, and fluorometrically using Qubit dsDNA HS Assay kits and a Qubit™ 1.0 Fluorometer (Invitrogen, Life Technologies).

All RNA-seq libraries, including single cell and bulk scleral tissues were sequenced on Hiseq 4000 System (Illumina) with 150 bp pair-end reads. After obtaining the raw sequencing data, Cutadapt tool (version 1.8) was used to remove the Illumina adapters and the sequences from Clontech Universal Primer Mix and Clontech SMARTer Oligonucleotides that remained in sequencing samples during the amplification process (7). Sequencing reads less than 70 bp were removed from further analysis. The trimmed sequences were then aligned to the mouse reference cDNA (GRCm38.rel79.cdna) from Ensembl using the kallisto tool (version 0.42.4) with default parameters (8). The expression level of each transcript was estimated using the transcripts per million (TPM) method (9).

To find highly variable genes among all scleral fibroblasts, we fitted the squared coefficient of variation (CV^2) as a function of the mean log transformed TPM with the parameterization $CV^2=\alpha_1/\mu+\gamma$, where μ was the average of TPM for each gene in all single-cells, α_1 and γ were the coefficients obtained by generalized linear model fitting (10). To minimize the skewing effect, genes with a mean TPM less than 1 were removed. Genes with an observed CV^2 larger than the expected CV^2 value calculated with the above function were considered to be highly variable.

We performed gene expression analysis of these highly variable genes. The differentially expressed genes (DEGs) were defined as those with a median TPM fold change of above 2 between the two scleral fibroblast populations, A1 and A2 (identified by hierarchical clustering of highly variable genes), and with a *P*-value (*t*-test) less than 0.05. We did not correct for multiple testing using the false discovery rate (FDR) as Rothman pointed out that "reducing the type I error for null associations increases the type II error for those associations that are not null…scientists should not be so reluctant to explore leads that may turn out to be wrong that they penalize themselves by missing possibly important findings" (11). Therefore, we adopted a relatively relaxed criterion that could outline more differentially expressed genes between the two distinct scleral cell populations. Given that ours was the first study to employ scRNA-seq to understand the mechanisms underlying myopia development, it was imperative that we made full use of the technology to avoid missing potentially important information. Besides, additional criteria for filtering the list of differentially expressed genes were in place to reduce the false positive rate. These included i) setting the median TPM among all cells to more than 1, ii) setting the squared coefficient of variation larger than expected, and iii) setting the minimum fold change of median TPM to more than 2. We carried out pathway analysis (Ingenuity Pathway Analysis, Qiagen. http://www.ingenuity.com/products/ipa) on these genes, which were also filtered for *P*-value and z-score. The expression of eight genes in the top three signaling pathways were validated separately. Collectively, various cutoff thresholds were used as part of the bioinformatic analysis.

To identify enriched gene sets in bulk tissue RNA-seq relative to scRNA-seq data, the gene set enrichment analysis was performed using the GSEA v3.0 software (12). Hypergeometric Optimization of Motif Enrichment (HOMER v4.9) was used to determine transcription factors possibly targeting the differentially expressed genes (13).

To identify the relevance of gene expression data in animal models to those in humans, we investigated the genes in the highly significant pathways identified from scRNA-seq data with known candidate genes of human myopia. Databases such as the Genome-Wide Association Study catalog and ClinVar (14, 15) were queried using the keywords “Myopia” and “Refractive Error” to extract the risk genes of human myopia. Genes obtained from study populations with “high grade myopia” or “pathologic myopia” were defined as pathologic myopia risk genes. The protein-protein interaction (PPI) data were downloaded from BioGRID (https://string-db.org/), and only genes that had data on the PPI network were used for further analysis. We obtained 145 myopia risk genes and 27 pathological myopia risk genes. A PPI network of myopia or pathologic myopia risk genes and those in the significant pathway from scRNA-seq was constructed through Cytoscape (http://cytoscape.org). Genes that interacted between these two datasets were shown in the network analysis. Enrichment analysis was done by hyper-geometric testing or 1,000 bootstrapping.

RT-PCR Validation of DEGs in the highly significant signaling pathways

After 2 days of FD, the murine scleral tissues (2 scleral tissues from mice were pooled together) were homogenized using a ball mill and total RNA was extracted with the RNeasy Fibrous Tissue Mini-kit (Qiagen) according to the manufacturer’s instructions. Total retinal RNA was extracted using TRIZOL™ reagent (Invitrogen). Scleral or retinal RNAs were subjected to reverse transcription with M-MLV Reverse Transcriptase (Promega) as previously described (16). The mRNA expression levels of 8 genes that were enriched in the top three signaling pathways (Table S4) were validated using RT-PCR (ABI 7500 Real-Time PCR System, Applied Biosystems), with specific primers (Table S8). The results were normalized to 18S rRNA.

Western blot analysis

After treatment, the scleras (4 scleral tissues from mice were pooled together) and retinas from mice or guinea pigs were separated and homogenized in radio immunoprecipitation assay (RIPA) lysis buffer (Beyotime, Shanghai, China) supplemented with 1 mM phenylmethanesulfonyl fluoride (PMSF) and Complete Mini (protease inhibitor cocktail). After centrifugation at 13,000xg for 10 min at 4°C, the supernatant was collected, and protein concentrations were determined using an Enhanced BCA Protein Assay Kit (Beyotime, Shanghai, China).

At the end of the designated periods, the cells were immediately placed on ice, washed with cold phosphate-buffered saline, and lysed with RIPA lysis buffer supplemented with 1 mM PMSF. The lysed cells were centrifuged at 13,000xg for 10 min at 4°C and the supernatant collected. The protein concentrations were determined using an Enhanced BCA Protein Assay Kit.

The expression levels of individual proteins were determined by western blot. Primary antibodies against collagen type I (1:1000, ab88147, Abcam), α-SMA (1:250, ab5694, Abcam), HIF-1α (1:800, 565924, BD Biosciences), eIF2α and P-eIF2α (1:800, 5324 and 3398, Cell Signaling Technology), mTOR and P-mTOR (1:800, 2983 and 5536, Cell Signaling Technology), paxillin (1:500, ab32084, Abcam), vinculin (1:500, ab129002, Abcam), α-tubulin (1.5:1000 for mice and 1:1000 for guinea pigs and cell culture, ab52866, Abcam), and β-actin (1:1250, A5441, Sigma) were used.

Densitometric analysis of the protein bands was conducted using Image J software (National Institutes of Health), and the values were normalized to the corresponding loading control, β-actin or α-tubulin. All western blots shown were representative of at least three independent experiments.

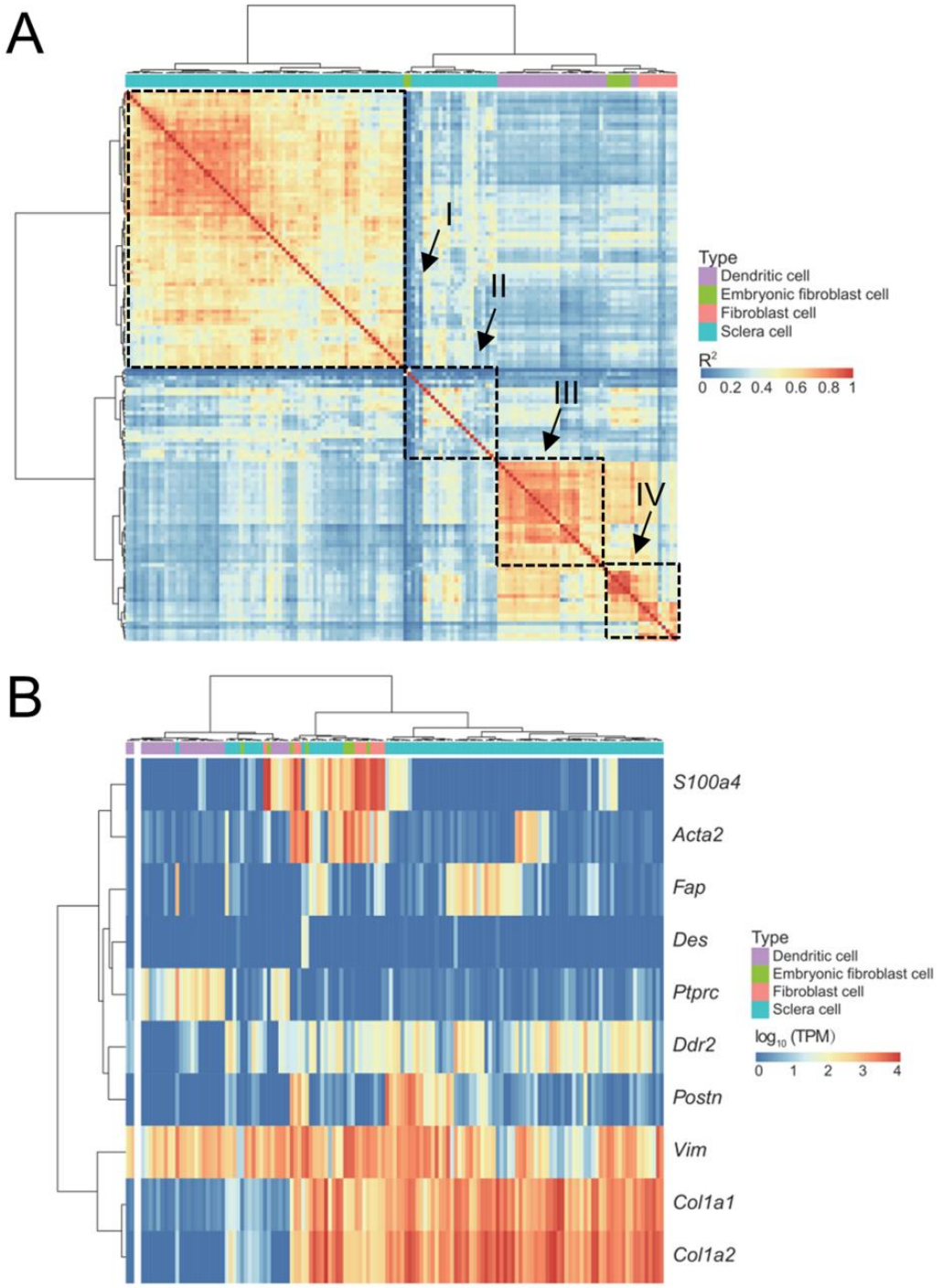

Figure S1. Purification of single scleral fibroblasts. (A) Unsupervised hierarchical clustering for cell-cell pairwise correlation based on gene expression profiles from our scleral single-cell data and the publicly available mouse scRNA-seq datasets (GSE60781 for dendritic cells, GSE47835 for embryonic fibroblasts, and GSE45719 for primary cultured fibroblasts). Dotted line frames represented 4 clusters in which single cells had similar profiles of correlation coefficients. The top-left axis represents single cells ordered by hierarchical clustering. Color codes represent different cellular origins, and the color scale represents R^2 values for pairwise correlation coefficients. **(B)** Clustering of single cells showing specific cellular markers. Nearly all fibroblasts highly expressed *Vim*, *Col1a1,* and *Col1a2*. Dendritic cells highly expressed *Ptprc*, a leukocyte marker. Color scale here represents $\log_{10}$ - transformed transcripts per million (TPM) values for each gene.

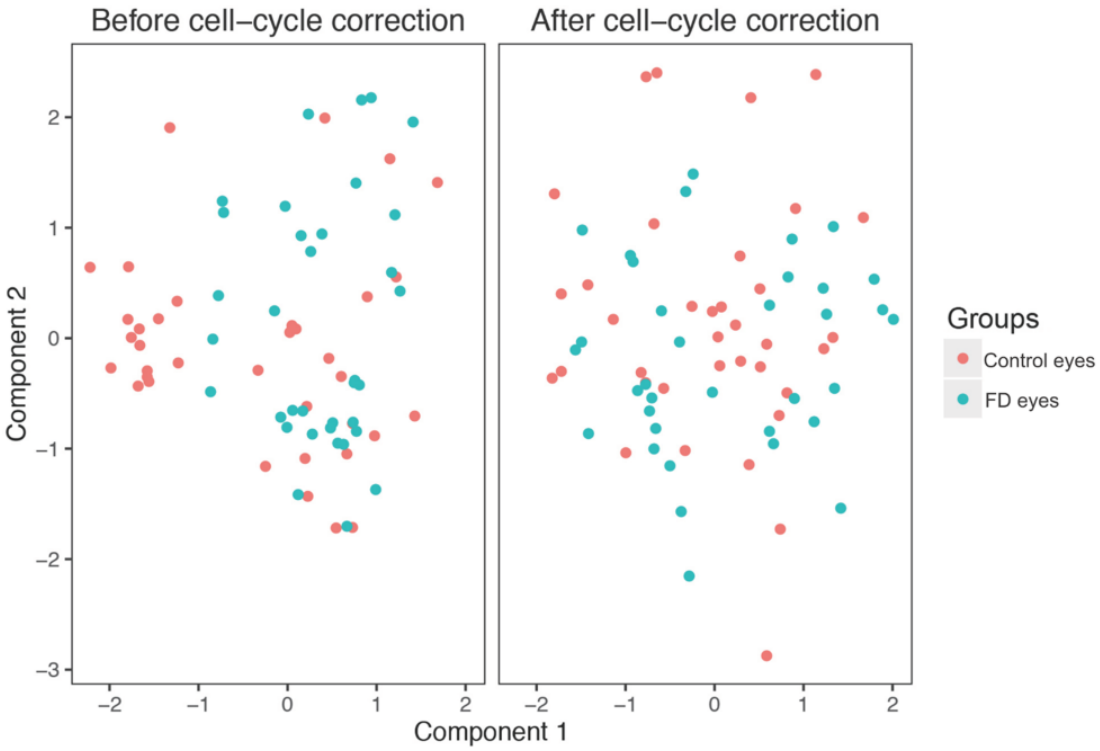

Figure S2. Principal component analysis for the remaining 71 cells from our scleral single-cells. Each dot represents a single cell from the 71 cells. Cell cycle is a major confounding factor that contributes to intercellular heterogeneity in scRNA-seq analyses. To determine if cell cycle contributed to the sub-clustering, we used 892 cell-cycle related genes to build a covariant matrix for normalizing the scRNA-seq data. We used principle component analysis to identify subgroupings. The results showed that single cells from form-deprived (blue dots) and their fellow control eyes (red dots) were randomly scattered. No subgrouping was observed either before (left panel) or after (right panel) cell-cycle adjustment. This indicates that cell cycle was not a major confounding factor in influencing the results of scRNA-seq.

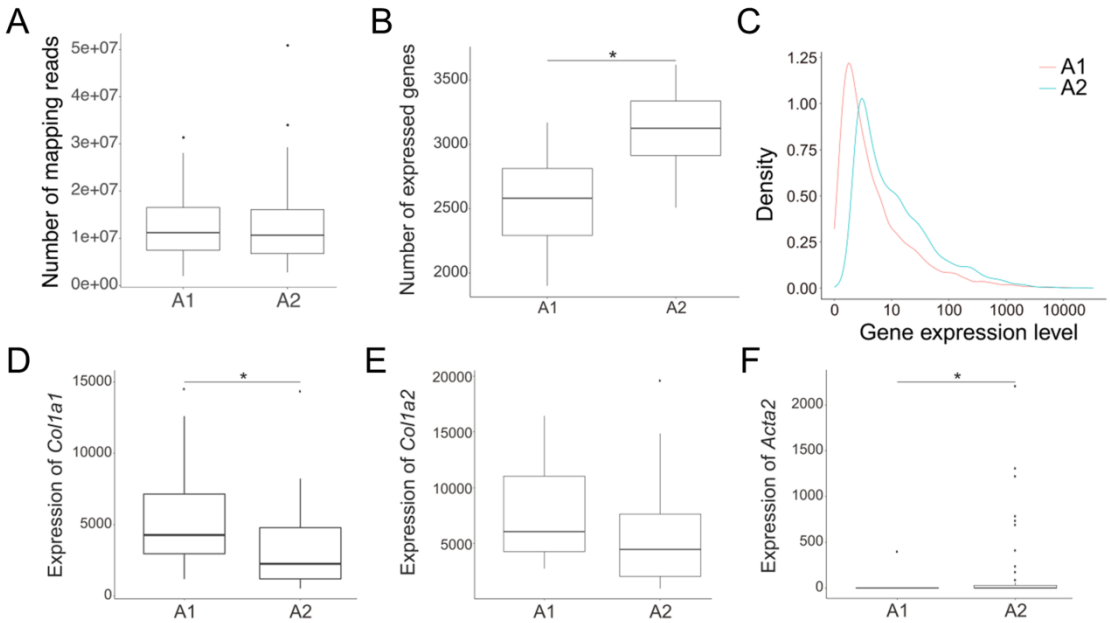

Figure S3. Characteristics of two fibroblast subpopulations. (A) Mapping reads, **(B)** the number of expressed genes and **(C)** their gene expression levels between A1 and A2 subpopulations are presented here. **(D)**, **(E)** and **(F)** show the levels of *Col1a1*, *Col1a2,* and *Acta2* between the two subpopulations, respectively. Data are expressed as medians (interquartile range), *P<0.05, *t*-test.

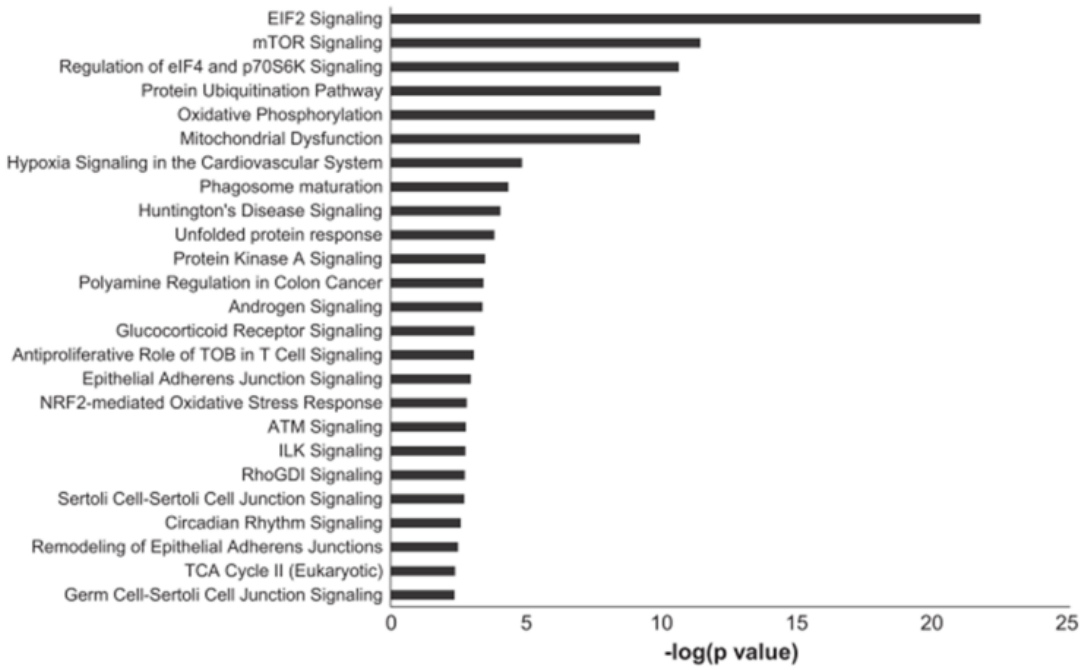

Figure S4. Pathway enrichment analysis for the differentially expressed genes between A1 and A2 subpopulations (A2 vs. A1). The pathway analysis was carried out using the Ingenuity Pathway Analysis tool, with an enrichment *P*-value cutoff of 0.01.

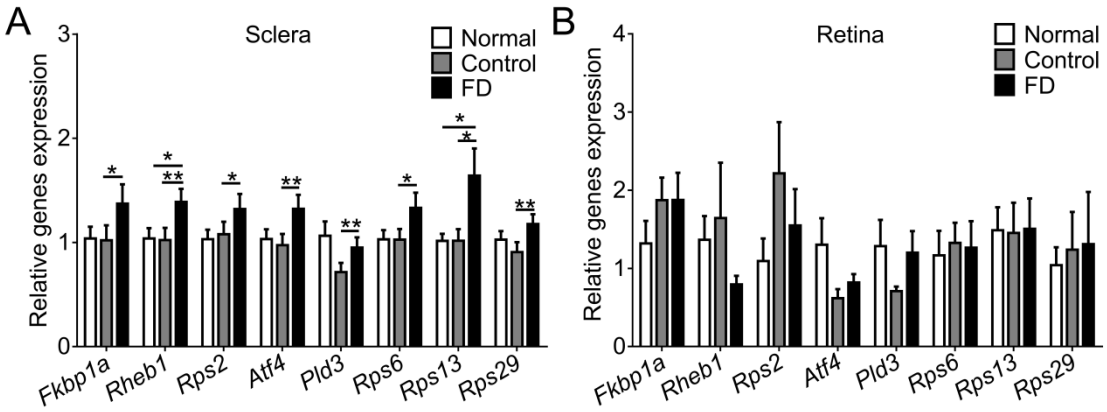

Figure. S5. Validation of genes in hypoxia-related pathways in myopia in mice. (A-B): Changes in mRNA levels of eight DEGs in the **(A)** sclera and **(B)** retina from mice after 2 days of FD (n=8). Data are expressed as mean ± SEM. *, *P*<0.05, **, *P*<0.01; Student's *t*-test.

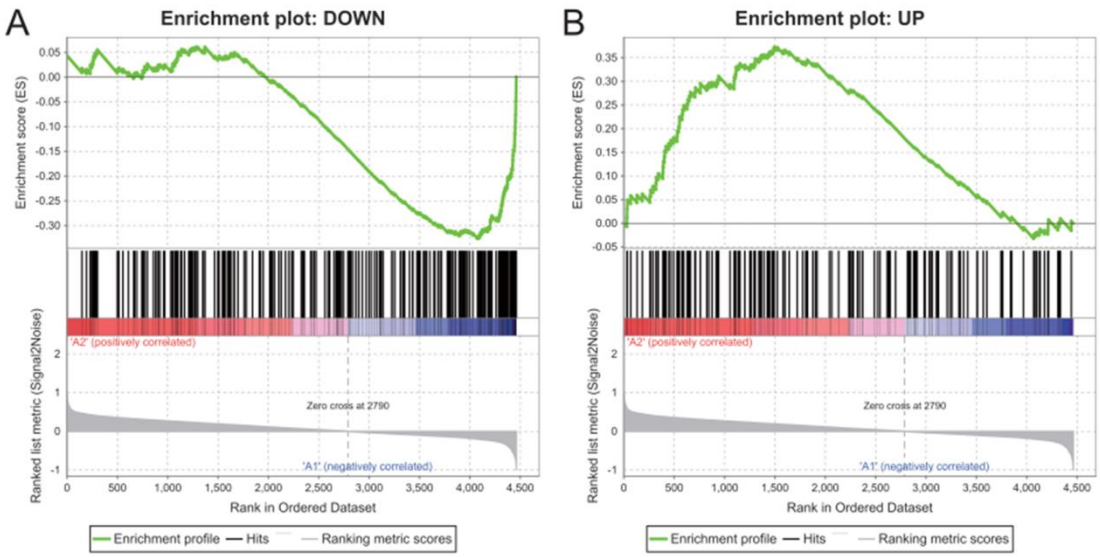

Figure S6. Comparison of single-cell data with that from bulk tissue using Gene Set Enrichment Analysis. For comparison of single-cell data with that of bulk tissue, we performed RNA-seq of the whole scleral tissue. **(A)** The 236 downregulated genes (FD vs. control) in scleral tissues were significantly enriched in the A1 gene set ($P<10^{-6}$). **(B)** On the other hand, the 150 upregulated genes in scleral tissues were enriched in the A2 gene set (P=0.0035). The higher enrichment scores indicate that the upregulated genes set tend to be highly expressed in the A2 population. The lower enrichment scores indicate the gene set tend to be highly expressed in the A1 population.

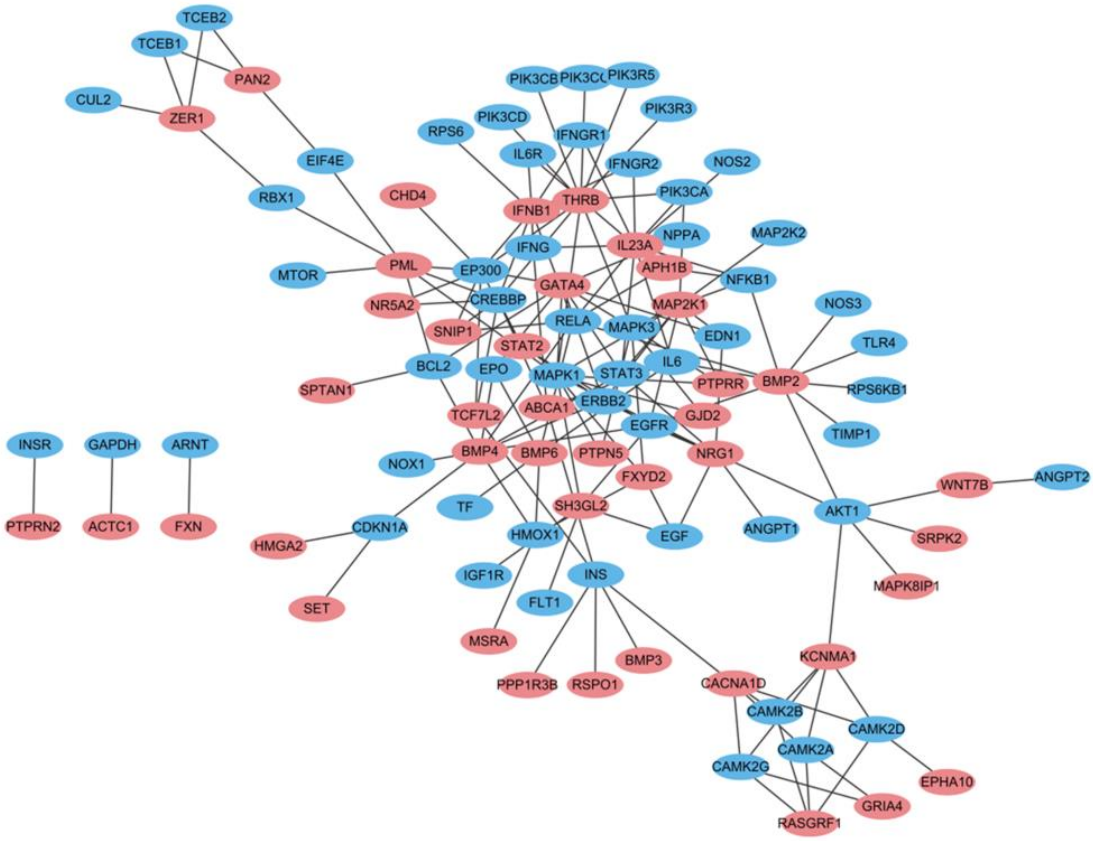

Figure S7. Relationship between human myopia risk genes and genes in the HIF-1α signaling pathway according to the PPI network. Among the 45 risk genes (red ovals), *THRB, IL23A, BMP2, GATA4, MAP2K1,* and *BMP4*, each having 9 or more connections with the genes in HIF-1α signaling pathway (blue ovals), indicate strong interactions with the hypoxia signaling pathway.

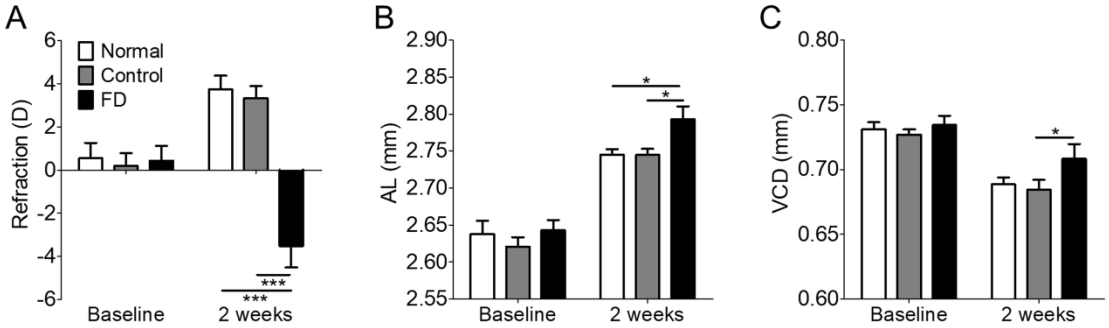

Figure S8. Monocular form-deprivation (FD) in mice. (A) refraction, **(B)** axial length (AL), and **(C)** vitreous chamber depth (VCD) from normal, control and FD eyes were measured at the baseline and 2 weeks after FD (n=16). Only right eyes from age-matched normal animals are shown. Data are expressed as mean ± SEM. **P*<0.05, ****P*<0.001, Student's *t*-test.

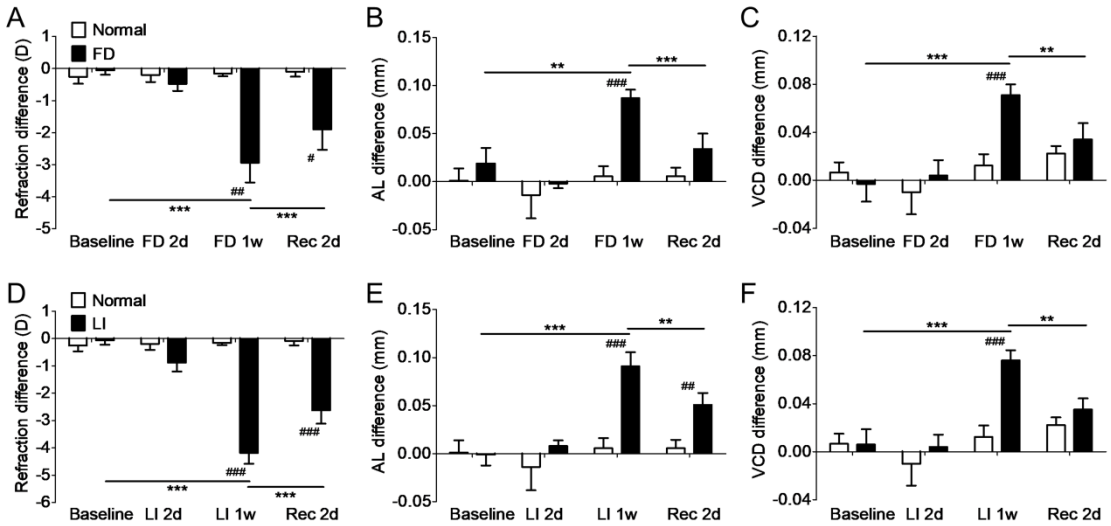

Figure S9. Myopia induction (FD or negative-lens induction, LI) in guinea pigs. Interocular differences (FD or LI eye minus control eye or right eye minus left eye) in **(A)** refraction, **(B)** axial length (AL), and **(C)** vitreous chamber depth (VCD) were repeatedly measured at baseline, 2 days and 1 week after FD, and 2 days after recovery from 1 week of FD. Interocular differences in **(D)** refraction, **(E)** AL, and **(F)** VCD were repeatedly measured at baseline, 2 days and 1 week after LI, and 2 days after recovery from 1 week of LI. FD and LI groups shared the same age-matched normal group (n=9-10). Five guinea pigs from each group were measured at 2 days. Data are expressed as mean ± SEM. ***P*<0.01, ****P*<0.001 between two timepoints; #*P*<0.05, ##*P*<0.01, ###*P*<0.001 between FD and normal groups or LI and normal groups; two-way repeated measures ANOVA with Bonferroni multiple comparisons.

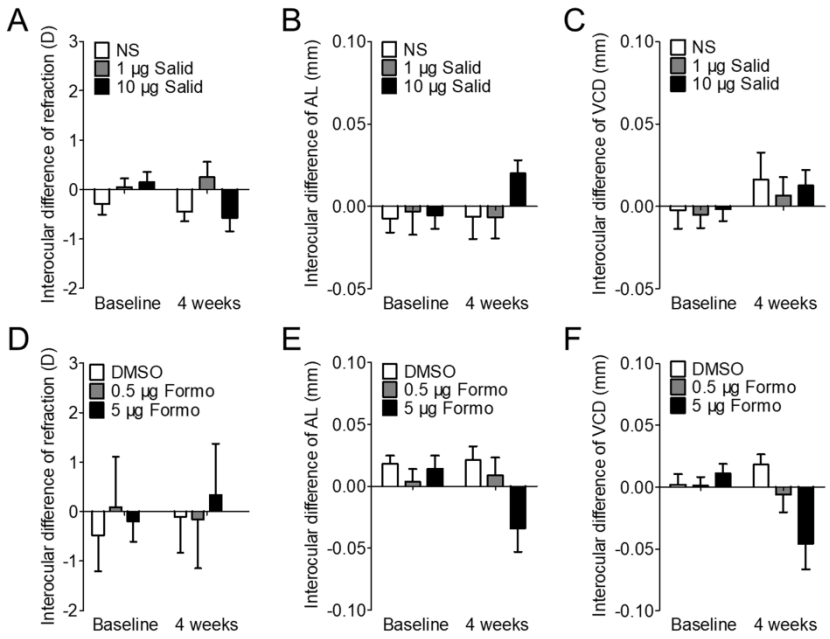

Figure S10. Effect of periocular administration of anti-hypoxic drugs on myopia development in normal guinea pigs. Interocular differences in refraction **(A)**, axial length **(B)** and vitreous chamber depth **(C)** in normal guinea pigs before and after 4 weeks of treatment with normal saline (NS, vehicle control, n=8), 1 μg per eye salidroside (Salid, n=6), or 10 μg per eye Salid (n=11). Interocular differences in refraction **(D)**, axial length **(E)**, vitreous chamber depth **(F)** in normal guinea pigs before and after 4 weeks of treatment with 0.1% dimethyl sulfoxide (DMSO, vehicle control, n=10), 0.5 μg per eye formononetin (Formo, n=8), or 5 μg per eye Formo (n=10). Interocular differences are presented as injected eye minus fellow uninjected eye. Data are expressed as mean ± SEM. *P<0.05, two-way repeated measures ANOVA with Bonferroni multiple comparisons. D: diopter; AL: axial length; VCD: vitreous chamber depth.

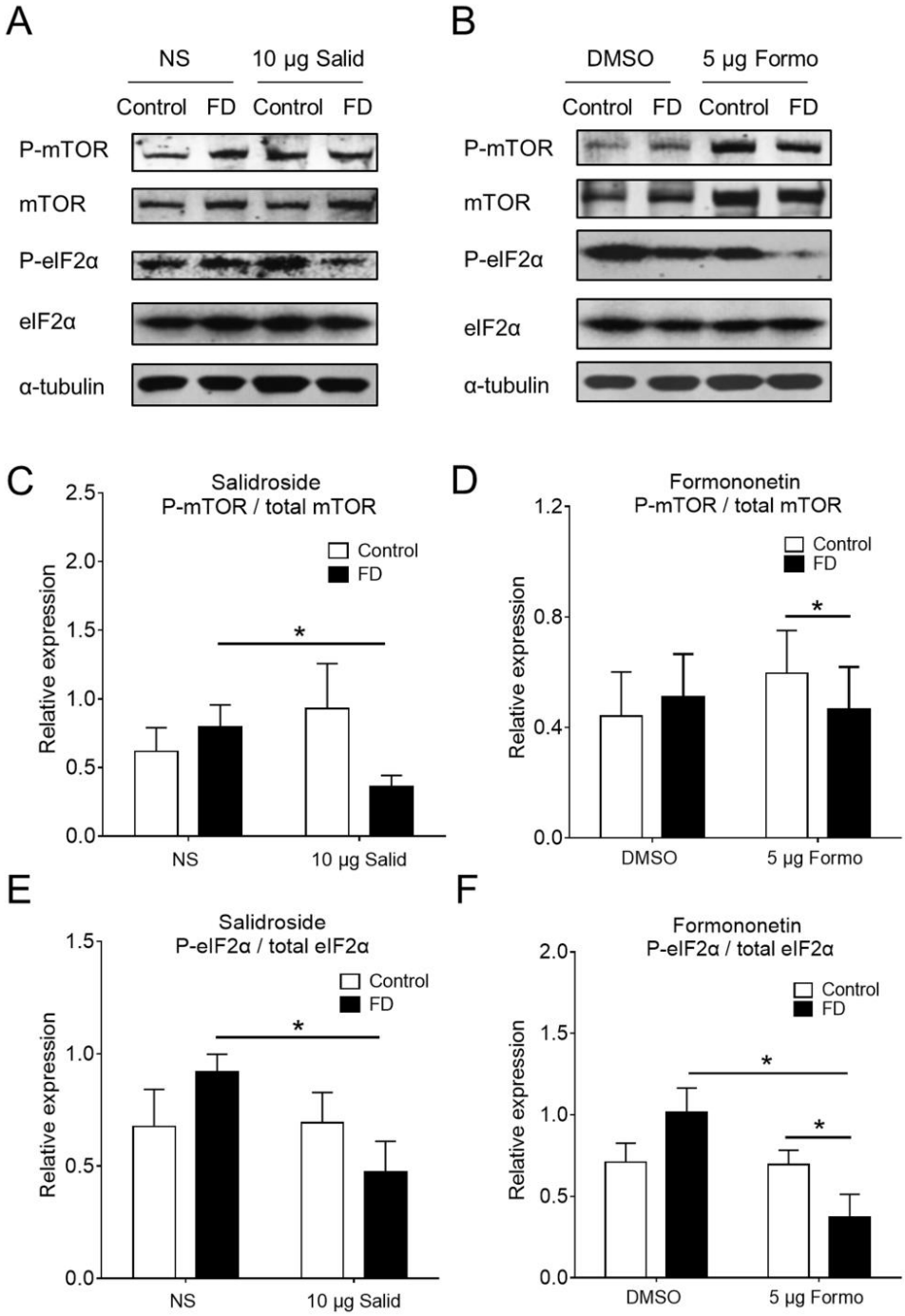

Figure S11. Phosphorylation levels of eIF2α and mTOR after treatment of FD guinea pigs with anti-hypoxic drugs. Levels of P-mTOR, mTOR, P-eIF2α, and eIF2α in sclera were detected by western blot after periocular injection of **(A)** 10 μg per eye salidroside (Salid) or **(B)** 5 μg per eye formononetin (Formo) for 4 weeks. **(C)** Ratio of P-eIF2α/total eIF2α after treatment with Salid (n=4). **(D)** Ratio of P-eIF2α/total eIF2α after treatment with Formo (n=4). **(E)** Ratio of P-mTOR/total mTOR after treatment with Salid (n=4). **(F)** Ratio of P-mTOR/total mTOR after treatment with Formo (n=4). Data are expressed as mean ± SEM. *, $P<0.05$, Student's *t*-test.

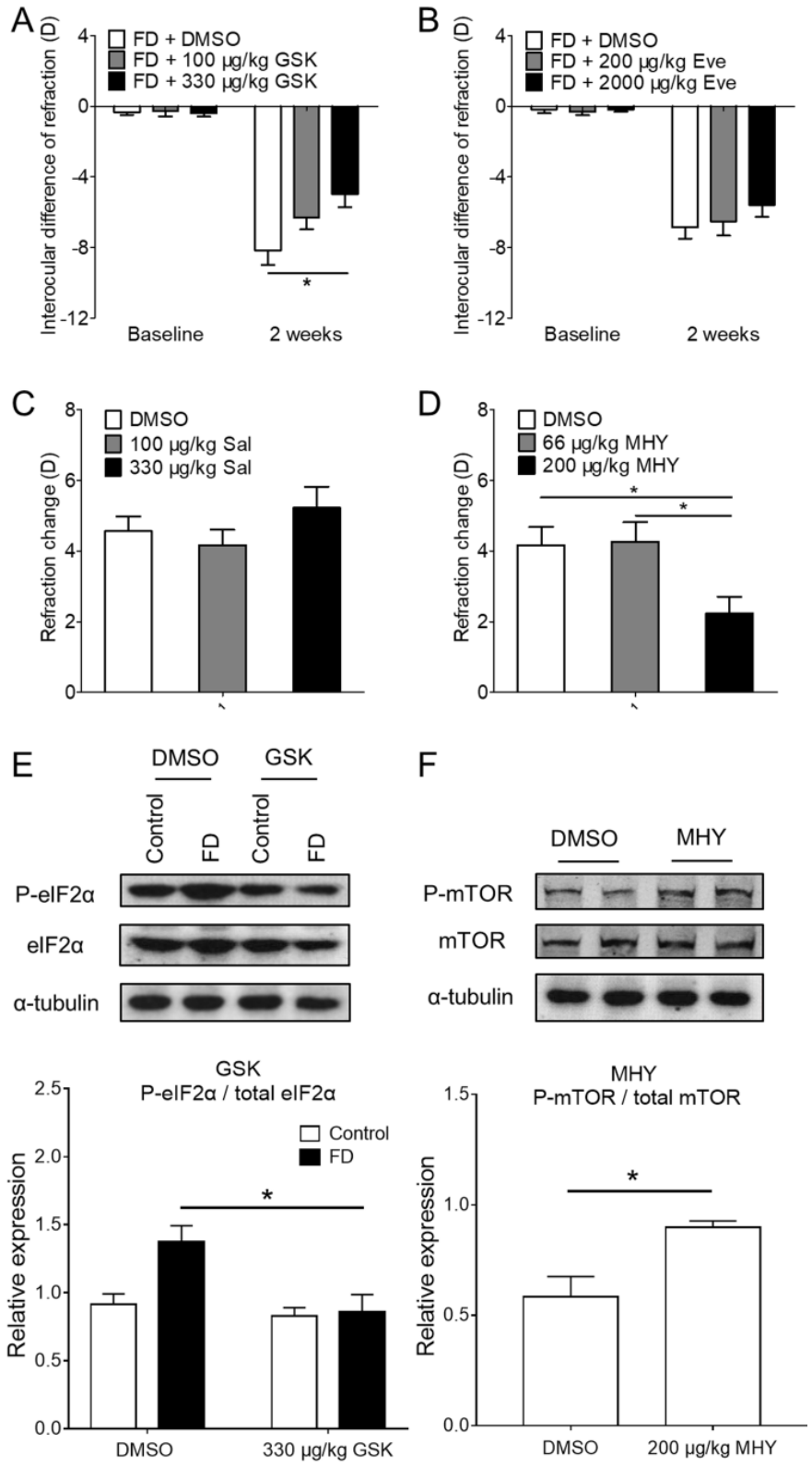

Figure S12. Effect of inhibition and activation of eIF2 and mTOR on refraction in FD mice. (A) Interocular difference (FD eye minus control eye) in refraction before and after 2 weeks of daily intraperitoneal injection of 1% DMSO (vehicle control, n=18), 100 μg/Kg GSK2606414 (GSK, an eIF2α phosphorylation inhibitor, n=22), or 330 μg/Kg body weight GSK (n=26). **(B)** Interocular difference in refraction in FD mice before and after 2 weeks of daily intraperitoneal injection of 1% DMSO (n=25), 200 μg/Kg everolimus (Eve, a mTOR inhibitor, n=28), or 2,000 μg/Kg body weight Eve (n=23). *, $P<0.05$, two-way repeated

measures ANOVA with Bonferroni multiple comparison. **(C)** Refractive change (post-treatment minus pre-treatment) in normal mice after 2 weeks of daily intraperitoneal injection of 1% DMSO (n=24), 100 μg/Kg salubrinal (Sal, an eIF2α dephosphorylation inhibitor, n=25), or 330 μg/Kg body weight Sal (n=24). **(D)** Refractive change in normal mice after 2 weeks of daily intraperitoneal injection of with 1% DMSO (n=24), 66 μg/Kg MHY1485 (MHY, a mTOR phosphorylation activator, n=25), or 200 μg/Kg body weight MHY (n=26). Changes in the right eyes of normal mice only are shown. *, $P<0.05$, one-way ANOVA with Bonferroni post hoc correction. **(E)** Ratios of P-eIF2α/total eIF2α in sclera after daily intraperitoneal injection with 330 μg/Kg GSK2606414 for 2 days (n=4). **(F)** Ratios of P-mTOR/total mTOR in sclera after daily intraperitoneal injection with 200 μg/Kg MHY for 2 days (n=4). Data are expressed as mean ± SEM. *, $P<0.05$, Student's *t*-test.

Table S1. Distribution of scleral single cells.

	Total cells		Excluded cells		Percentage of excluded cells	
Batch ID	control	FD	control	FD	control	FD
b1	21	1	6	0	28%	0%
b2	14	14	2	1	14%	7%
b3	9	23	0	6	0%	26%
b4	/	11	/	7	/	63%

The symbol "/" means that single cell capture was not performed with the control eye in this batch.

Table S2. Quality of each single-cell RNA-sequencing data from our study.

ID	Remaining reads*	Mapped reads$	Mapping ratio	Exon ratio**	Cells used in analysis#
0109-F-C74	26,151,656	19,994,270	76.46%	76.85%	yes
0109-F-C91	23,019,146	17,402,210	75.60%	73.49%	yes
0109-F-C31	19,164,872	13,737,049	71.68%	75.72%	yes
1025-T-C37	17,723,838	12,562,108	70.88%	74.00%	yes
1025-F-C63	14,880,162	10,540,555	70.84%	74.18%	yes
1025-T-C95	39,500,046	27,706,090	70.14%	69.60%	yes
1025-F-C41	33,515,688	23,297,353	69.51%	70.26%	yes
0109-F-C45	45,147,582	31,339,899	69.42%	72.98%	yes
0110-F-C93	23,610,260	16,110,808	68.24%	80.03%	yes
0109-T-C59	2,952,550	1,996,328	67.61%	59.36%	yes
0109-F-C12	9,293,414	6,213,709	66.86%	81.30%	yes
1025-T-C66	24,353,036	16,047,342	65.89%	70.69%	yes
1025-T-C65	20,366,462	13,389,874	65.74%	64.87%	yes
0110-T-C50	15,653,046	10,195,156	65.13%	71.73%	yes
1025-T-C85	42,326,836	27,532,014	65.05%	61.63%	yes
1025-T-C92	36,758,732	23,861,642	64.91%	61.81%	yes
1025-F-C94	22,221,064	14,292,675	64.32%	67.58%	yes
1025-F-C45	53,153,576	33,973,862	63.92%	60.48%	yes
1025-T-C81	24,207,398	15,274,060	63.10%	61.18%	yes
0109-F-C11	22,499,012	14,148,305	62.88%	70.13%	yes
1025-T-C29	19,546,206	12,240,999	62.63%	59.41%	yes
0110-T-C89	10,071,854	6,181,640	61.38%	68.18%	yes
1025-T-C28	48,164,390	29,285,792	60.80%	56.40%	yes
1025-F-C44	83,923,458	50,849,947	60.59%	64.71%	yes
0110-T-C91	17,732,096	10,713,630	60.42%	69.46%	yes
0110-T-C84	16,921,870	10,216,761	60.38%	76.11%	yes
1106-T-C91	46,866,888	28,086,582	59.93%	63.42%	yes
1025-T-C25	17,823,214	10,650,253	59.75%	61.75%	yes
0110-F-C74	11,285,498	6,682,123	59.21%	72.57%	yes
1025-T-C59	43,047,438	25,476,406	59.18%	51.89%	yes
0109-F-C28	14,068,854	8,311,475	59.08%	61.34%	yes
0110-T-C49	9,295,690	5,475,088	58.90%	84.05%	yes
0110-T-C59	12,145,026	7,148,308	58.86%	67.77%	yes

0110-F-C90	8,717,550	5,124,588	58.78%	77.27%	yes
1025-F-C89	20,459,896	11,982,524	58.57%	54.58%	yes
1025-T-C60	21,479,022	12,562,643	58.49%	53.42%	yes
0110-F-C25	12,477,914	7,271,032	58.27%	71.95%	yes
1025-T-C93	42,874,602	24,945,260	58.18%	57.46%	yes
0109-F-C87	43,617,978	24,986,420	57.28%	52.09%	yes
1025-T-C17	34,075,954	19,369,097	56.84%	49.87%	yes
0109-F-C62	19,702,772	11,165,125	56.67%	59.43%	yes
0110-T-C93	13,492,440	7,642,426	56.64%	66.58%	yes
1025-T-C43	22,509,294	12,722,778	56.52%	54.79%	yes
1025-T-C73	38,468,118	21,665,469	56.32%	49.58%	yes
0109-F-C55	26,406,646	14,842,118	56.21%	51.77%	yes
0110-F-C51	19,118,242	10,719,071	56.07%	63.30%	yes
0110-F-C24	12,043,032	6,737,410	55.94%	65.89%	yes
0109-F-C18	18,234,058	10,131,581	55.56%	51.97%	yes
0109-F-C92	9,087,064	5,031,180	55.37%	53.87%	yes
0110-T-C77	10,128,554	5,586,662	55.16%	64.16%	yes
1025-F-C81	20,494,104	11,300,064	55.14%	52.47%	yes
0110-T-C64	13,884,664	7,641,870	55.04%	70.45%	yes
1025-F-C48	19,348,418	10,623,552	54.91%	53.08%	yes
1025-T-C89	18,455,636	10,093,667	54.69%	50.13%	yes
1025-F-C61	48,621,686	26,506,110	54.51%	47.67%	yes
0109-F-C36	14,462,918	7,854,676	54.31%	52.05%	yes
0110-F-C40	9,529,974	5,140,237	53.94%	67.66%	yes
0109-F-C78	8,894,854	4,795,644	53.91%	47.65%	yes
0110-F-C59	16,467,034	8,858,212	53.79%	60.72%	yes
0110-F-C95	12,874,224	6,777,994	52.65%	67.76%	yes
1106-T-C79	21,411,022	11,212,202	52.37%	49.28%	yes
0110-F-C78	12,115,222	5,974,958	49.32%	69.85%	yes
0110-T-C57	7,457,826	3,671,233	49.23%	58.70%	yes
0110-T-C47	16,006,912	7,797,024	48.71%	61.93%	yes
0109-F-C58	34,104,262	16,233,899	47.60%	43.28%	yes
0110-F-C83	8,018,504	3,794,107	47.32%	59.26%	yes
0110-T-C18	10,609,368	5,016,841	47.29%	79.17%	yes
1106-T-C82	18,727,540	8,699,742	46.45%	41.55%	yes
0110-T-C33	6,124,948	2,791,233	45.57%	66.51%	yes
0110-F-C68	15,105,804	6,652,828	44.04%	71.72%	yes
1106-T-C73	12,685,740	5,312,410	41.88%	36.90%	yes

0109-F-C04	15,102,110	9,304,711	61.61%	58.84%	no
0109-F-C13	44,739,882	21,914,286	48.98%	41.64%	no
0109-F-C47	50,836,828	27,699,873	54.49%	45.91%	no
0109-F-C52	10,961,894	5,730,116	52.27%	51.27%	no
0109-F-C60	16,926,110	9,266,806	54.75%	56.89%	no
0109-F-C84	11,209,024	6,690,255	59.69%	61.45%	no
0110-F-C73	7,214,854	3,137,726	43.49%	51.86%	no
0110-F-C75	15,286,456	9,000,623	58.88%	73.23%	no
0110-T-C51	10,172,096	6,364,279	62.57%	98.38%	no
1025-T-C21	15,177,962	8,099,388	53.36%	44.60%	no
1025-T-C46	31,149,404	12,484,143	40.08%	43.69%	no
1025-T-C52	44,477,796	19,371,530	43.55%	41.48%	no
1025-T-C55	11,107,296	5,165,638	46.51%	51.18%	no
1025-T-C71	18,422,898	8,211,983	44.57%	36.47%	no
1025-T-C79	26,636,604	14,196,889	53.30%	44.72%	no
1106-T-C19	28,563,520	13,340,813	46.71%	41.41%	no
1106-T-C26	32,088,568	20,966,558	65.34%	69.16%	no
1106-T-C39	16,528,864	5,679,423	34.36%	28.99%	no
1106-T-C77	19,680,120	9,558,239	48.57%	48.03%	no
1106-T-C83	24,701,168	10,782,764	43.65%	41.03%	no
1106-T-C94	21,095,206	8,819,072	41.81%	38.68%	no
1106-T-C96	14,146,208	5,655,085	39.98%	35.52%	no

"-T-" and "-F-" in ID column represent "FD eye" and "fellow control eye" respectively from the sclera of monocular FD mice.

* Remaining reads after adapter trimming and primer cutting;

$ Reads mapped to GRCm38.rel79.cdna;

** Ratio of exon reads based on mapping to mouse reference genome GRCm38 by STAR;

The 71 cells used in subgrouping analysis.

Table S3. Single-cells from Gene Expression Omnibus (GEO) datasets.

GEO dataset	Sample	Run
GSE60781	CDP_1	SRR1558744
GSE60781	CDP_2	SRR1558745
GSE60781	CDP_3	SRR1558746
GSE60781	CDP_4	SRR1558747
GSE60781	CDP_5	SRR1558748
GSE60781	CDP_6	SRR1558749
GSE60781	CDP_7	SRR1558750
GSE60781	CDP_8	SRR1558751
GSE60781	CDP_9	SRR1558752
GSE60781	CDP_10	SRR1558753
GSE60781	PreDC_1	SRR1558840
GSE60781	PreDC_2	SRR1558841
GSE60781	PreDC_3	SRR1558842
GSE60781	PreDC_4	SRR1558843
GSE60781	PreDC_5	SRR1558844
GSE60781	PreDC_6	SRR1558845
GSE60781	PreDC_7	SRR1558846
GSE60781	PreDC_8	SRR1558847
GSE60781	PreDC_9	SRR1558848
GSE60781	PreDC_10	SRR1558849
GSE60781	MDP_1	SRR1558936
GSE60781	MDP_2	SRR1558937
GSE60781	MDP_3	SRR1558938
GSE60781	MDP_4	SRR1558939
GSE60781	MDP_5	SRR1558940
GSE60781	MDP_6	SRR1558941
GSE60781	MDP_7	SRR1558942
GSE60781	MDP_8	SRR1558943
GSE60781	MDP_9	SRR1558944
GSE60781	MDP_10	SRR1558945
GSE45719	fibroblast_13_CxB	SRR1041755
GSE45719	fibroblast_14_CxB	SRR1041756
GSE45719	fibroblast_15_CxB	SRR1041757
GSE45719	fibroblast_16_CxB	SRR1041758
GSE45719	fibroblast_17_BxC	SRR1041759
GSE45719	fibroblast_19_BxC	SRR1041760

GSE45719	fibroblast_20_BxC	SRR1041761
GSE45719	fibroblast_21_BxC	SRR1041762
GSE45719	fibroblast_22_BxC	SRR1041763
GSE45719	fibroblast_9_CxB	SRR1041764
GSE47835	MEF1	SRR1267517
GSE47835	MEF2	SRR1267518
GSE47835	MEF3	SRR1267519
GSE47835	MEF4	SRR1267520
GSE47835	MEF5	SRR1267521
GSE47835	MEF6	SRR1267522
GSE47835	MEF7	SRR1267523
GSE47835	MEF8	SRR1267524

Table S4. Differentially expressed genes enriched in the top three hypoxia-related signaling pathways.

Signaling pathway	Genes
EIF2 signaling	*Rpl24, Rpl22, Rps23, Rpl35a, Rpl7a, Rps11, Rps28, Rps20, Eif4g2, Rpl13,* ***Rps13****, Rps9, Rpl19,* ***Rps2****, Rps3, Rps5, Rpl31, Rpl18, Pabpc1, Rps19, Rpl3, Rpl17, Rps10, Rps21,* ***Rps29****, Rpl28, Eif3m, Fau,* ***Rps6****, Rpl15, Rpl27, Rps26, Rps27a, Rpl37, Rps25, Rps15a, Eif3l, Rps14, Rplp0*
mTOR signaling	*Rps23,* ***Fkbp1a****, Rps11, Rps28, Rps20, Eif4g2,* ***Rps13****, Rps9,* ***Rps2****, Rps5, Rps3, Rps19,* ***Rheb****,* ***Pld3****, Rps10, Rhoj, Rps21,* ***Rps29****, Fau, Eif3m,* ***Rps6****, Rnd3, Rps26, Rps27a, Rps25, Rps15a, Eif3l, Rps14*
Hypoxia signaling in the cardiovascular system	*Ube2l3, Jun, Nfkbia, Hsp90ab1, Sumo1, Creb3, Ube2v1,* ***Atf4****, Ube2l6, Ube2f*

The genes listed underwent a significant change in expression patterns in transitioning from the A1 to A2 subpopulations (*t*-tests with $P<0.05$ and fold change of median TPM > 2 or<0.5). The genes in bold font were validated at the bulk tissue level by RT-PCR.

Table S5. Potential transcription factors involved in A1 to A2 transition.

Motif	P-value	Best Match
	1e-12	Tlx?(NR)/NPC-H3K4me1-ChIP-Seq (GSE16256)/Homer(0.698)
	1e-12	RUNX1(Runt)/Jurkat-RUNX1-ChIP-Seq(GSE29180)/Homer(0.605)
	1e-12	NFY(CCAAT)/Promoter/Homer(0.651)
	1e-11	Srebp1a(bHLH)/HepG2-Srebp1a-ChIP-Seq(GSE31477)/Homer(0.608)
	1e-11	Bapx1(Homeobox)/VertebralCol-Bapx1-ChIP-Seq(GSE36672)/Homer(0.597)
	1e-10	Znf263(Zf)/K562-Znf263-ChIP-Seq (GSE31477)/Homer(0.634)
	1e-10	Crx/MA0467.1/Jaspar(0.620)
	1e-10	BMYB(HTH)/Hela-BMYB-ChIP-Seq (GSE27030)/Homer(0.676)
	1e-10	Smad4(MAD)/ESC-SMAD4-ChIP-Seq (GSE29422)/Homer(0.723)
	1e-10	Foxh1(Forkhead)/hESC-FOXH1-ChIP-Seq(GSE29422)/Homer(0.706)

	1e-9	E2F6/MA0471.1/Jaspar(0.619)
	1e-9	E2F6(E2F)/Hela-E2F6-ChIP-Seq (GSE31477)/Homer(0.681)
	1e-9	n-Myc(bHLH)/mES-nMyc-ChIP-Seq (GSE11431)/Homer(0.808)
	1e-9	REST/MA0138.2/Jaspar(0.580)
	1e-9	LIN54/MA0619.1/Jaspar(0.717)
	1e-9	PB0127.1_Gata6_2/Jaspar(0.599)
	1e-8	Sox5/MA0087.1/Jaspar(0.872)
	1e-8	NFY(CCAAT)/Promoter/Homer(0.791)
	1e-8	COUP-TFII(NR)/Artia-Nr2f2-ChIP-Seq(GSE46497)/Homer(0.655)
	1e-8	Sox2/MA0143.3/Jaspar(0.720)
	1e-8	PB0139.1_Irf5_2/Jaspar(0.651)
	1e-8	ESRRB/MA0141.3/Jaspar(0.597)

	1e-8	RUNX2(Runt)/PCa-RUNX2-ChIP-Seq(GSE33889)/Homer(0.639)
	1e-8	PB0179.1_Sp100_2/Jaspar(0.593)
	1e-8	Hoxa9/MA0594.1/Jaspar(0.621)
	1e-8	Ahr::Arnt/MA0006.1/Jaspar(0.671)
	1e-8	PB0124.1_Gabpa_2/Jaspar(0.675)
	1e-8	PB0194.1_Zbtb12_2/Jaspar(0.702)
	1e-8	GLIS1/MA0735.1/Jaspar(0.636)
	1e-8	HIF-1a(bHLH)/MCF7-HIF1a-ChIP-Seq(GSE28352)/Homer(0.817)
	1e-7	PB0179.1_Sp100_2/Jaspar(0.669)
	1e-7	PB0134.1_Hnf4a_2/Jaspar(0.689)
	1e-7	PB0156.1_Plagl1_2/Jaspar(0.558)

	1e-5	ZNF189(Zf)/HEK293-ZNF189.GFP-ChIP-Seq(GSE58341)/Homer(0.597)
	1e-5	Sox17/MA0078.1/Jaspar(0.677)
	1e-4	Nr2e3/MA0164.1/Jaspar(0.705)

Potential transcription factors of the differentially expressed genes (DEGs) were identified by analyzing the promoter sequences. Overrepresented sequence motifs were extracted and used to perform hypergeometric distribution tests.

Motif: overrepresented sequences in the promoter of DEGs.

P-value: significant level for hypergeometric test. Transcription factors with enrichment *P*<1e-4 are listed.

Best Match: transcription factors binding to the motif.

Table S6. Risk genes of human myopia and pathologic myopia.

Catalogue	Risk genes
Myopia	*BRF2, CYP26A1, IL23A, GNB3, MAPK8IP1, PEX16, COL10A1, KCNJ2, BMP4, SLC14A2, RDH5, MIP, PGBD1, FXYD6, SIX3, COL8A1, PZP, APH1B, VIPR2, DNAH9, ASPA, HAT1, ZIC5, PML, NUF2, CAPN9, ERLIN2, LRRC4C, GRIA4, BMP3, BMP6, PTPRR, MYO5B, PDE11A, PCDH1, CACNA1D, IL17RB, GJD2, ACTC1, ZER1, PKN3, FXYD2, ZNF281, ALPPL2, SNIP1, DNALI1, LRFN5, CPSF2, MAP2K1, ANTXR2, CTNND2, PPP1R3B, GPD2, GLE1, RBFOX1, GLS2, SLC35C1, MSRA, CA8, METAP1D, DSCAML1, STAT2, CDCA8, CD55, CHDH, DIS3L, MYO1D, FBN1, CNDP2, NT5DC1, SIX6, RAB11FIP1, NPLOC4, GATA4, CDKN3, DHX15, ACTR8, WNT7B, TNFSF13, KCNQ5, FILIP1L, THRB, RSPO1, SPTBN1, NRG1, CHD4, SEMA4F, PTPN5, GK2, RGR, TOX, COL6A1, NR5A2, NFIA, SET, WDR34, SPTAN1, EPHA10, GNL2, DENND1A, BICC1, FRMPD2, ABCA1, DLG2, PCCA, ZIC2, RORB, FXN, CAMKMT, BMP2, IFNB1, ADAMTSL1, SH3GL2, NLN, MIPEP, PTPRN2, CHRNG, SRPK2, TFAP2B, TBC1D23, APOF, PCBP3, HMGA2, NRXN1, KCNMA1, SHISA6, CHD7, PHF21A, LAMA2, PAN2, ZNF469, CLSTN2, PBX1, RASGRF1, GABRR1, OR4A47, STIM2, SELK, STAU2, TJP2, PDE10A, PCDH7, TCF7L2, TIMELESS, BLID.*
Pathologic myopia	*PHA42, SCO2, VIPR2, DNAH9, ASPA, SLC39A5, PML, CAPN9, BMP6, PCDH1, NCAPH2, CTNND2, PPP1R3B, PRIMPOL, MSRA, GATA4, DHX15, SPTBN1, CHD4, SEMA4F, DENND1A, ABCA1, MIPEP, PTPRN2, SRPK2, CLSTN2, LRPAP1.*

Table S7. Differentially expressed genes (DEGs) that interact with risk genes of human myopia.

Catalogue	DEGs
With risk genes of myopia	*Abat, Acin1, Acta2, Actn1, Actn4, Ap2s1, Apc, Aplp2, Apoe, Arglu1, Ash2l, Atf3, Atp1b3, Atrx, Bhlhe40, Bhlhe41, Cct2, Cct4, Cfl1, Ckap5, Cpsf6, Ctcf, Cthrc1, Cul1, Eps15, Fkbp1a, Fzd7, Glul, Gnai3, Gng12, Gps2, H2afv, Hbp1, Hnrnpf, Hnrnpr, Hsp90ab1, Hspa2, Hspa8, Hspa9, Ilk, Ing3, Ipo4, Itgb5, Jak1, Jun, Kcnma1, Klhl9, Kpna1, Lepr, Magoh, Map2k3, Med13, Mef2a, Mfap5, Mier1, Msrb3, Ndufb7, Nedd8, Nfe2l2, Nfkbia, Nop58, Npr2, Nr1d1, Nudc, Pabpc1, Papola, Pcbp1, Pcna, Per3, Pld3, Pls3, Plxnb2, Polr1d, Polr2f, Prkar1a, Ptbp1, Rap1a, Rbx1, Rpl23a, Rpl3, Rps27a, Rps6, Rqcd1, Sdhb, Sec11a, Sec13, Selm, Sfrp2, Sirt1, Skiv2l2, Slu7, Smad3, Smad4, Smc4, Snrpd1, Snw1, Spcs2, Sptan1, Srsf9, Ssrp1, Stx12, Sumo1, Synj1, Tagln2, Tcf4, Tgif1, Timp1, Tuba1a, Ubc, Vmp1, Wls, Xaf1, Xbp1, Zeb1, Zfhx4.*
With risk genes of pathologic myopia	*Acin1, Actn1, Actn4, Apoe, Arglu1, Atrx, Cox11, Fkbp1a, Glul, Ilk, Jun, Magoh, Mef2a, Msrb3, Nop58, Pabpc1, Plxnb2, Polr1d, Rap1a, Rbx1, Sec11a, Sirt1, Skiv2l2, Slu7, Smad3, Smad4, Smc4, Snw1, Spcs2, Sptan1, Srsf9, Ssrp1, Stx12, Sumo1, Surf1, Tgif1, Tuba1a, Ubc, Zeb1, Zfhx4.*

Table S8. Real-time PCR primers used in this study.

Target	Forward primer	Backward primer
18s rRNA	CGGACACGGACAGGATTGAC	TGCCAGAGTCTCGTTCGTTATC
Fkbp1a	GATTCCTCTCGGGACAGAAACA	GACCCACACTCATCTGGGCTA
Rheb1	GGTCTGTGGGAAAGTCCTCAT	GGTGAACGTGTTCTCTATGGTT
Rps2	GGGGCTCGTGGAGGTAAAG	TCTCAGACTCCTTAATGGGCAG
Atf4	CCTGAACAGCGAAGTGTTGG	TGGAGAACCCATGAGGTTTCAA
Pld3	AAGCCCAAACTGATGTACCAG	CCTTCCATGCCTCGATTTCATT
Rps6	AAGAGTGGAAGGGTTATGTGGT	GGTCAGAACACCTTGCTTCAT
Rps13	TCCCTCCCAGATAGGTGTAATCC	TCCTTTCTGTTCCTCTCAAGGT
Rps29	GTCTGATCCGCAAATACGGG	AGCCTATGTCCTTCGCGTACT

References

1. Schaeffel F, Burkhardt E, Howland HC, Williams RW (2004) Measurement of refractive state and deprivation myopia in two strains of mice. *Optom Vis Sci* 81(2):99-110.
2. Zhou X, et al. (2008) Biometric measurement of the mouse eye using optical coherence tomography with focal plane advancement. *Vision Res* 48(9):1137-1143.
3. Lu F, et al. (2006) Axial myopia induced by a monocularly-deprived facemask in guinea pigs: A non-invasive and effective model. *Exp Eye Res* 82(4):628-636.
4. Lu F, et al. (2009) Axial myopia induced by hyperopic defocus in guinea pigs: A detailed assessment on susceptibility and recovery. *Exp Eye Res* 89(1):101-108.
5. Jiang L, et al. (2009) Spontaneous axial myopia and emmetropization in a strain of wild-type guinea pig (Cavia porcellus). *Invest Ophthalmol Vis Sci* 50(3):1013-1019.
6. Wu AR, et al. (2014) Quantitative assessment of single-cell RNA-sequencing methods. *Nat Methods* 11(1):41-46.
7. Martin M (2011) Cutadapt removes adapter sequences from high-throughput sequencing reads. *EMBnet. journal* 17(1):pp. 10-12.
8. Bray NL, Pimentel H, Melsted P, Pachter L (2016) Near-optimal probabilistic RNA-seq quantification. *Nat Biotechnol* 34(5):525-527.
9. Li B, Ruotti V, Stewart RM, Thomson JA, Dewey CN (2010) RNA-Seq gene expression estimation with read mapping uncertainty. *Bioinformatics* 26(4):493-500.
10. Buettner F, et al. (2015) Computational analysis of cell-to-cell heterogeneity in single-cell RNA-sequencing data reveals hidden subpopulations of cells. *Nat Biotechnol* 33(2):155-160.
11. Rothman KJ (1990) No adjustments are needed for multiple comparisons. *Epidemiology* 1(1):43-46.
12. Subramanian A, et al. (2005) Gene set enrichment analysis: a knowledge-based approach for interpreting genome-wide expression profiles. *Proc Natl Acad Sci U S A* 102(43):15545-15550.
13. Heinz S, et al. (2010) Simple combinations of lineage-determining transcription factors prime cis-regulatory elements required for macrophage and B cell identities. *Mol Cell* 38(4):576-589.
14. Welter D, et al. (2014) The NHGRI GWAS Catalog, a curated resource of SNP-trait associations. *Nucleic Acids Res* 42(Database issue):D1001-1006.
15. Landrum MJ, et al. (2016) ClinVar: public archive of interpretations of clinically relevant variants. *Nucleic Acids Res* 44(D1):D862-868.
16. Zhou X, et al. (2012) Experimental murine myopia induces collagen type Ialpha1 (COL1A1) DNA methylation and altered COL1A1 messenger RNA expression in sclera. *Mol Vis* 18:1312-1324.